

# Frequency Dependent Electrical Transport in the Integer Quantum Hall Effect

Ludwig Schweitzer

## 1 Introduction

It is well established to view the integer quantum Hall effect (QHE) as a sequence of quantum phase transitions associated with critical points that separate energy regions of localised states where the Hall-conductivity  $\sigma_{xy}$  is quantised in integer units of  $e^2/h$  (see, e.g., [1,2]). Simultaneously, the longitudinal conductivity  $\sigma_{xx}$  gets unmeasurably small in the limit of vanishing temperature and zero frequency. To check the inherent consequences of this theoretical picture, various experiments have been devised to investigate those properties that should occur near the critical energies  $E_n$  assigned to the critical points. For example, due to the divergence of the localisation length  $\ell(E) \propto |E - E_n|^{-1}$ , the width of the longitudinal conductivity peaks emerging at the transitions is expected to exhibit power-law scaling with respect to temperature, system size, or an externally applied frequency.

High frequency Hall-conductivity experiments, initially aimed at resolving the problem of the so-called low frequency breakdown of the QHE apparently observed at 1 MHz, were successfully carried out at microwave frequencies ( $\sim 33$  MHz) [3]. The longitudinal ac conductivity was also studied to obtain some information about localisation and the formation of Hall plateaus in the frequency ranges 100 Hz to 20 kHz [4] and 50{600 MHz [5]. Later, frequency dependent transport has been investigated also in the Gigahertz frequency range below 15 GHz [6,7] and above 30 GHz [8,9,10].

Dynamical scaling has been studied in several experiments, some of which show indeed power law scaling of the  $\sigma_{xx}(\omega)$  peak width as expected,  $\propto \omega^{-1}$  [6,11,12], whereas others do not [7]. The exponent  $\nu = (z)^{-1}$  contains both the critical exponent of the localisation length and the dynamical exponent  $z$  which relates energy and length scales,  $E \propto L^{-z}$ . The value of  $\nu = 2.35 \pm 0.03$  is well known from numerical calculations [13,14], and it also coincides with the outcome of a finite size scaling experiment [15]. However, it is presently only accepted as true that  $z = 2$  for non-interacting particles, and  $z = 1$  if Coulomb electron-electron interactions are present [16,17,18,19,20]. Therefore, a theoretical description of the ac conductivities would clearly contribute to a better understanding of dynamical scaling at quantum critical points.

Legal metrology represents a second area where a better knowledge of frequency dependent transport is highly desirable because the ac quantum Hall effect is applied for the realization and dissemination of the impedance standard and the unit of capacitance, the farad. At the moment the achieved relative uncertainty at a frequency of 1 kHz is of the order  $10^{-7}$  which still is at least one order of magnitude too large [21,22,23,24]. It is unclear whether the observed deviations from the quantised dc value are due to external influences like capacitive and inductive couplings caused by the leads and contacts. Alternatively, the measured frequency effects that make exact quantisation impossible could be already inherent in an ideal non-interacting two-dimensional electron gas in the presence of disorder and a perpendicular magnetic field. Of course, applying a finite frequency  $\omega$  will lead to a finite  $\sigma_{xx}(\omega)$  and in turn will influence the quantisation of  $\sigma_{xy}(\omega)$ , but it remains to be investigated how large the deviation will be.

Theoretical studies of the ac conductivity in quantum Hall systems started in 1985 [25] when it was shown within a semiclassical percolation theory that for finite frequencies the longitudinal conductivity is not zero, thus influencing the quantisation of the Hall-conductivity. The quantum mechanical problem of non-interacting electrons in a 2d disordered system in the presence of a strong perpendicular magnetic field  $B$  was tackled by Apel [26] using a variational method. Applying an instanton approximation and coming to the high field limit, i.e., restricting to the lowest Landau level (LLL), an analytical solution for the real part of the frequency dependent longitudinal conductivity could be presented,  $\sigma_{xx}(\omega) / \omega^2 \ln(1/\omega^2)$ , a result that should hold if the Fermi energy lies deep down in the lower tail of the LLL.

Generalising the above result, both real and imaginary parts of the frequency dependent conductivities were obtained in a sequence of papers by Viehweger and Efetov [27,28,29]. The Kubo conductivities were determined by calculating the functional integrals in super-symmetric representation near non-trivial saddle points. Still, for the final results the Fermi energy was restricted to lie within the energy range of localised states in the lower tail of the lowest Landau band and, therefore, no proposition for the critical regions at half fillings could be given. The longitudinal conductivity was found to be

$$\sigma_{xx}(\omega) = c \omega^2 \ln^b(1/\omega^2) \approx \omega^2 2 l_B^2 \rho(E_F); \quad (1)$$

with the density of states  $\rho(E_F)$ , and two unspecified constants  $b$  and  $c$  [27]. The real part of the Hall-conductivity in the same limit was proposed as

$$\sigma_{yx}(\omega) = e^2 \hbar (h/\omega)^2 8 l_B^2 n_e; \quad (2)$$

where  $l_B = \sqrt{\hbar/(eB)}$  is the magnetic length,  $\omega^2 = \omega^2 l_B^2$  is the second moment of the white noise disorder potential distribution with disorder strength  $\omega^2$ , and  $n_e$  denotes the electron density. The deviation due to frequency of the Hall-conductivity from its quantised dc plateau value can be perceived from

an approximate expression proposed by Viehweger and Efetov [29] for the 2nd plateau, e.g., for filling factor  $\nu = 2$ ,

$$\sigma_{xx}(\omega) = e^2 \hbar \frac{2}{1 + \frac{\omega^2}{\omega_c^2}} \frac{2\hbar}{\omega_c} \left( \frac{\omega}{\omega_c} \right)^2 : \quad (3)$$

Again,  $\omega_c$  is a measure of the disorder strength describing the width of the disorder broadened Landau band, and  $\omega_c = eB/\hbar m_e$  is the cyclotron frequency with electron mass  $m_e$ . According to (3), due to frequency a deviation from the quantised value becomes apparent even for integer filling.

Before reviewing the attempts which applied numerical methods to overcome the limitations that had to be conceded in connexion with the position of  $E_F$  in the analytical work, and to check the permittiveness of the approximations made, it is appropriate here to mention a result for the hopping regime. Polyakov and Shklovskii [30] obtained for the dissipative part of the ac conductivity a relation which, in contrast to (1), is linear in frequency  $\omega$ ,

$$\sigma_{xx}(\omega) = K \omega : \quad (4)$$

This expression has recently been used to successfully describe experimental data [31]. Here,  $\xi$  is the localisation length,  $\epsilon$  the dielectric constant, and the pre-factor is  $K = 1/6$  in the limit  $\hbar \omega \ll k_B T$ . Also, the frequency scaling of the peak width  $\omega_p$  was proposed within the same hopping model [30].

Turning now to the numerical approaches which were started by Gammel and Brenig who considered the low frequency anomalies and the finite size scaling of the real part of the conductivity peak  $\sigma_{xx}(\omega; L_y)$  at the critical point of the lowest Landau band [32]. For these purposes the authors utilised the random Landau model in the high field limit (lowest Landau band only) [1,13] and generalised Maackinnon's recursive Green function method [33] for the evaluation of the real part of the dynamical conductivity. In contrast to the conventional quadratic Drude-like behaviour the peak value decayed linearly with frequency,  $\sigma_{xx}(\omega) = \frac{0}{\omega} \text{const} \cdot \omega$ , which was attributed to the long time tails in the velocity correlations which were observed also in a semi-classical model [34,35]. The range of this unusual linear frequency dependence varied with the spatial correlation length of the disorder potentials. A second result concerns the scaling of  $\sigma_{xx}(\omega; L_y)$  at low frequencies as a function of the system width  $L_y$ ,  $\sigma_{xx}(\omega; L_y^2) / (\omega L_y^2)^2 = \text{const}$ , where  $\text{const} = 2 - D(2) = 0.36 - 0.06$  [32] is related to the multi-fractal wave functions [36,37,38,39], and to the anomalous diffusion at the critical point with  $\alpha = 0.38$  [40] and  $D(2) = 1.62$  [41].

The frequency scaling of the  $\sigma_{xx}(\omega)$  peak width was considered numerically for the first time in a paper by Avishai and Luck [42]. Using a continuum model with spatially correlated Gaussian disorder potentials placed on a square lattice, which then was diagonalised within the subspace of functions pertaining to the lowest Landau level, the real part of the dissipative conductivity was evaluated from the Kubo formula involving matrix elements

of the velocity of the guiding centres [43]. This is always necessary in single band approximations because of the vanishing of the current matrix elements between states belonging to the same Landau level. As a result, a broadening of the conductivity peak was observed and from a finite size scaling analysis a dynamical exponent  $z = 1.19 \pm 0.13$  could be extracted using  $\nu = 2.33$  from [13]. This is rather startling because it is commonly believed that for non-interacting systems  $z$  equals the Euclidean dimension of space which gives  $z = d = 2$  in the QHE case.

A different theoretical approach for the low frequency behaviour of the  $\rho_{xx}(\omega)$  peak has been pursued by Jug and Ziegler [44] who studied a Dirac fermion model with an inhomogeneous mass [45] applying a non-perturbative calculation. This model leads to a non-zero density of states and to a finite bandwidth of extended states near the centre of the Landau band [46]. Therefore, the ac conductivity as well as its peak width do neither show power-law behaviour nor do they vanish in the limit  $\omega \rightarrow 0$ . This latter feature of the model has been asserted to explain the linear frequency dependence and the finite intercept at  $\omega = 0$  observed experimentally for the width of the conductivity peak by Balaban et al. [7], but, up to now, there is no other experiment showing such a peculiar behaviour.

## 2 Preliminary considerations { basic relations

In the usual experiments on two-dimensional systems a current  $I_x(\omega)$  is driven through the sample of length  $L_x$  and width  $L_y$ . The voltage drop along the current direction,  $U_x(\omega)$ , and that across the sample,  $U_y(\omega)$ , are measured from which the Hall-resistance  $R_H(\omega) = U_y(\omega)/I_x(\omega) = \rho_{xy}(\omega)$  and the longitudinal resistance  $R_x(\omega) = U_x(\omega)/I_x(\omega) = \rho_{xx}(\omega)L_x/L_y$  are obtained, where  $\rho_{xy}$  and  $\rho_{xx}$  denote the respective resistivities. To compare with the theoretically calculated conductivities one has to use the relations in the following, only in Corbino samples  $\rho_{xx}(\omega)$  can be experimentally detected directly.

The total current through a cross-section,  $I_x(\omega) = \int_0^{L_y} j_k(\omega; r) dy$ , is determined by the local current density  $j_k(\omega; r)$  which constitutes the response to the applied electric field

$$j_k(\omega; r) = \int_{-\infty}^{\infty} \int_{-\infty}^{\infty} \rho_{ku}(\omega; r; r^0) E_u(\omega; r^0) d^2 r^0 : \quad (5)$$

The nonlocal conductivity tensor is particularly important in phase-coherent mesoscopic samples. Usually, for the investigation of the measured macroscopic conductivity tensor one is not interested in its spatial dependence. Therefore, one relies on a local approximation and considers the electric field to be effectively constant. This leads to Ohm's law  $j = \sigma E$  from which the resistance components are simply given by inverting the conductivity tensor

b

$$\frac{\rho_{xx}}{\rho_{yy}} = \frac{1}{\frac{\rho_{xx}}{\rho_{yy}} + \frac{\rho_{xy}}{\rho_{yx}}} \quad \rho_{xy} = \rho_{yx} \quad (6)$$

For an isotropic system we have  $\rho_{xx} = \rho_{yy}$  and  $\rho_{xy} = \rho_{yx}$  which in case of zero frequency gives the well known relations

$$\rho_{xx} = \frac{\rho_{xx}}{2} + \frac{\rho_{xy}}{2}; \quad \rho_{xy} = \frac{\rho_{xy}}{2} + \frac{\rho_{xy}}{2} \quad (7)$$

From experiment one knows that whenever  $\rho_{xy}$  is quantised  $\rho_{xx}$  gets unsaturable small which in turn means that  $\rho_{xx} \neq 0$  and  $\rho_{xy} = 1/\rho_{yx}$ . Therefore, to make this happen one normally concludes that the corresponding electronic states have to be localised.

In the presence of frequency this argument no longer holds because electrons in localised states do respond to an applied time dependent electric field giving rise to an alternating current. Also, both real and imaginary parts have to be considered now

$$\rho_{xx}(\omega) = \rho_{xx}^R(\omega) + i \rho_{xx}^I(\omega); \quad \rho_{xy}(\omega) = \rho_{xy}^R(\omega) + i \rho_{xy}^I(\omega) \quad (8)$$

Assuming an isotropic system, the respective tensor components of the ac resistivity  $\rho_{uv}(\omega) = \rho_{uv}^R(\omega) + i \rho_{uv}^I(\omega)$  with  $u, v = x, y$  can be written as

$$\rho_{uv}^R(\omega) = \frac{\rho_{vu}^R \left( \frac{\rho_{xx}^R}{2} + \frac{\rho_{xy}^R}{2} \right) + 2 \rho_{vu}^I \left( \frac{\rho_{xx}^R}{2} \frac{\rho_{xx}^I}{2} + \frac{\rho_{xy}^R}{2} \frac{\rho_{xy}^I}{2} \right)}{\left( \frac{\rho_{xx}^R}{2} + \frac{\rho_{xy}^R}{2} \right)^2 + 4 \left( \frac{\rho_{xx}^R}{2} \frac{\rho_{xx}^I}{2} + \frac{\rho_{xy}^R}{2} \frac{\rho_{xy}^I}{2} \right)^2} \quad (9)$$

$$\rho_{uv}^I(\omega) = \frac{\rho_{vu}^I \left( \frac{\rho_{xx}^R}{2} + \frac{\rho_{xy}^R}{2} \right) + 2 \rho_{uv}^R \left( \frac{\rho_{xx}^R}{2} \frac{\rho_{xx}^I}{2} + \frac{\rho_{xy}^R}{2} \frac{\rho_{xy}^I}{2} \right)}{\left( \frac{\rho_{xx}^R}{2} + \frac{\rho_{xy}^R}{2} \right)^2 + 4 \left( \frac{\rho_{xx}^R}{2} \frac{\rho_{xx}^I}{2} + \frac{\rho_{xy}^R}{2} \frac{\rho_{xy}^I}{2} \right)^2} \quad (10)$$

with the abbreviations  $\frac{\rho_{xx}^R}{2} = \left( \frac{\rho_{xx}^R}{2} \right)^2 = \left( \frac{\rho_{xx}^I}{2} \right)^2$  and  $\frac{\rho_{xy}^R}{2} = \left( \frac{\rho_{xy}^R}{2} \right)^2 = \left( \frac{\rho_{xy}^I}{2} \right)^2$ .

### 3 Model and Transport theory

We describe the dynamics of non-interacting particles moving within a two-dimensional plane in the presence of a perpendicular magnetic field and random electrostatic disorder potentials by a lattice model with Hamiltonian

$$H = \sum_r w_r \hat{c}_r^\dagger \hat{c}_r + \sum_{\langle r, r' \rangle} V_{rr'} \hat{c}_r^\dagger \hat{c}_{r'} \quad (11)$$

The random disorder potentials associated with the lattice sites are denoted by  $w_r$  with probability density distribution  $P(w_r) = 1/W$  within the interval  $[-W/2; W/2]$ , where  $W$  is the disorder strength, and the  $\hat{c}_i$  are the lattice base vectors. The transfer terms

$$V_{rr'} = V \exp \left( -i \mathbf{e} \cdot \mathbf{r} \right) \quad (12)$$

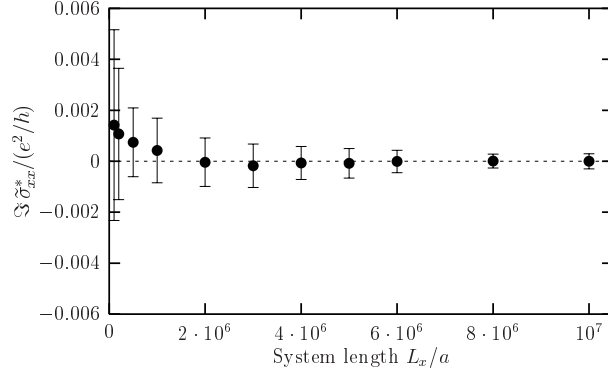


Fig.1. Disorder averaged imaginary part of  $\sigma_{xx}(E; i\eta)$  at energy  $E = V = 3.35$ , frequency  $\hbar\omega = V = 0.001$ , and  $\eta = V = 0.0008$  as a function of sample length  $L_x = N a$ . The system width is  $L_y = a = 32$  and the number of realisations amounts to 29 for  $L_x = a = 5 \cdot 10^5$  and to 8 for larger lengths

which connect only nearest neighbours on the lattice, contain the influence of the applied magnetic field via the vector potential  $A(x) = (0; Bx; 0)$  in their phase factors.  $V$  and the lattice constant  $a$  define the units of energy and length, respectively.

The electrical transport is calculated within linear response theory using the Kubo formula which allows to determine the time dependent linear conductivity from the current matrix elements of the unperturbed system

$$\sigma_{uv}(E_F; T; i\eta) = \frac{e^2}{\hbar} \frac{1}{\text{Tr } \hat{v}_u(E_F - H) \hat{v}_v(E_F + \hbar\omega - H)} \int_{-\infty}^{\infty} dE \frac{f(E) - f(E + \hbar\omega)}{i\eta} \quad (13)$$

where  $f(E) = (\exp[(E - E_F)/(k_B T)] + 1)^{-1}$  is the Fermi function. The area of the system is  $A = L_x L_y$ ,  $\hat{v}_u = i\hbar[H; u]$  signifies the  $u$ -component of the velocity operator, and  $(E + \hbar\omega - H) = i\eta(2)(G^{i\dagger}(E) - G^{i\dagger}(E))$ , where  $G^{i\dagger}(E) = (E + \hbar\omega - i\eta)I - H)^{-1}$  is the resolvent with imaginary frequency  $i\eta$  and unit matrix  $I$ .

For finite systems at temperature  $T = 0$  K, ensuring the correct order of limits for size and imaginary frequency  $i\eta$ , one gets with  $\eta = \omega + 2i\eta = \hbar$

$$\sigma_{uv}(E_F; i\eta) = \lim_{\eta \rightarrow 0} \lim_{\omega \rightarrow 1} \frac{e^2}{\hbar} \frac{1}{\hbar\omega} \int_{E_F - \hbar\omega}^{E_F} dE \text{Tr} \left[ (\hbar\omega)^2 [uG^{i\dagger} vG] + (\hbar\omega)^2 [uG^{i\dagger} vG^+] + 2i\eta [uv(G^{i\dagger} - G)] \right] \quad (14)$$

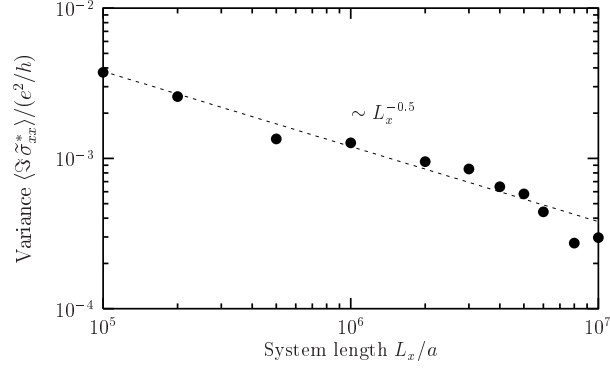


Fig. 2. The variance of  $\langle \Re \tilde{\sigma}_{xx}^* \rangle / (e^2/h)$  versus system length  $L_x$  calculated for the averages shown in Fig. 1 exhibiting an empirical power-law  $L_x^{-0.5}$

$$\begin{aligned}
 &= \lim_{\hbar \rightarrow 0} \lim_{\epsilon \rightarrow 1} \frac{e^2}{h} \frac{1}{h!} \int_{E_F - \hbar!}^{E_F} \int_{E_F - \hbar!}^{E_F} e_{uv}(E; \epsilon; \hbar; L_x; L_y) dE \\
 &+ \int_{E_F - \hbar!}^{E_F} e_{uv}(E; \epsilon; \hbar; L_x; L_y) dE : \quad (15)
 \end{aligned}$$

One can show that the second integral with the limits  $(E_F - \hbar!; E_F)$  does not contribute to the real part of  $e_{uv}(E_F; \epsilon!)$  because the kernel is identical zero, but we were not able to prove the same also for the imaginary part. Therefore, using the recursive Green function method explained in the next section, we numerically studied  $e_{uv}(E; \epsilon; \hbar; L_x; L_y)$  and found it to become very small only after disorder averaging. As an example we show in Fig. 1 the dependence of  $\langle \Re \tilde{\sigma}_{xx}^* \rangle$ , averaged over up to 29 realisations, on the length of the system for a particular energy  $E = V = 3.35$  and width  $L_y = a = 32$ . Also the variance of  $\langle \Re \tilde{\sigma}_{xx}^* \rangle$  gets smaller with system length following an empirical power law  $(L_x/a)^{-0.5}$  (see Fig. 2). In what follows we neglect the second integral for the calculation of the imaginary parts of the conductivities and assume that only the contribution of the first one with limits  $(E_F - \hbar!; E_F)$  matters. Of course, one has to be particularly careful even if the kernel is very small because with increasing disorder strength the energy range that contributes to the integral (finite density of states) tends to infinity. Therefore, a rigorous proof for the vanishing of this integral kernel is highly desirable.

#### 4 Recursive Green function method

A very efficient method for the numerical investigation of large disordered chains, strips and bars that are assembled by successively adding on slice at a time has been pioneered by Mackinnon [47]. This iterative technique relies on

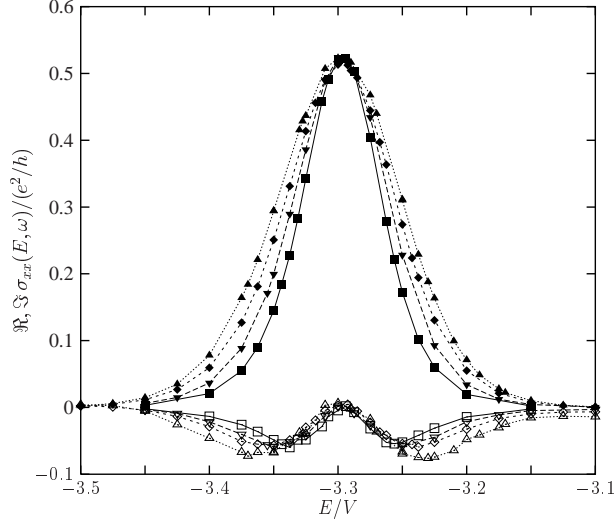


Fig.3. The real and imaginary parts of  $\sigma_{xx}(E; \omega)$  as a function of energy and frequency  $\hbar\omega = V = 2 \cdot 10^4$  (■),  $5 \cdot 10^4$  (□),  $1 \cdot 10^3$  (◆),  $2 \cdot 10^3$  (◻). For comparison, the cyclotron frequency is  $\hbar\omega_c = 1.57V$  for  $B = 1/8$  which was chosen for the magnetic flux density. The disorder strength is  $W = V = 1$  and the maximal system width amounts to  $L_y = a = 96$  with periodic boundary conditions applied.

the property that the Hamiltonian  $H^{(N+1)}$  of a lattice system containing  $N+1$  slices, each a lattice constant  $a$  apart, can be decomposed into parts that describe the system containing  $N$  slices,  $H^{(N)}$ , the next slice added,  $H_{N+1;N+1}$ , and a term that connects the last slice to the rest,  $H_N^0 = H_{N;N+1} + H_{N+1;N}$ . Then the corresponding resolvent is formally equivalent to the Dyson equation  $G = G_0 + G_0 \hat{V} G$  where the 'unperturbed'  $G_0$  represents the direct sum of  $H^{(N)}$  and  $H_{N+1;N+1}$ , and  $\hat{V}$  corresponds to the 'interaction'  $H_N^0$ . The essential advantage of this method is the fact that, for a fixed width  $L_y$ , the system size is increased in length adding slice by slice, whereas the size of the matrices to be dealt with numerically remains the same [47,48].

A number of physical quantities like localisation length [49,50,51,52], density of states [51,53], and some dc transport coefficients [33,54,55] have been calculated by this technique over the years. Also, this method was implemented for the evaluation of the real part of the ac conductivity in 1d [56,57] and 2d systems [32,58,59]. Furthermore it included also the real and imaginary parts of the Hall- and the imaginary part of the longitudinal conductivity in quantum Hall systems were also successfully accomplished [60,61,62].

The iteration equations of the resolvent matrix acting on the subspace of such slices with indices  $i, j \leq N$  in the  $N$ -th iteration step can be written as

$$G_{ij}^{!; (N+1)} = G_{ij}^{!; (N)} + G_{i;N}^{!; (N)} H_{N;N+1} G_{N+1;N+1}^{!; (N+1)} H_{N+1;N} G_{N;j}^{!; (N)}$$



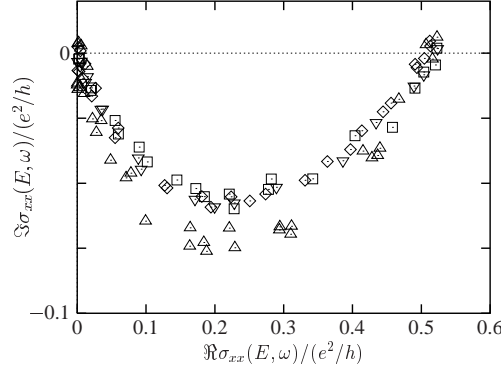


Fig.4. The imaginary part of  $\sigma_{xx}(E; \omega)$  as a function of the real part. Data are taken from Fig.3

$$\begin{aligned}
 G_{N+1, N+1}^{!; ;(N+1)} &= [E + h! - i\omega] I - H_{N+1, N+1} - H_{N+1, N} G_{N, N}^{!; ;(N)} H_{N, N+1}]^{-1} \\
 G_{i, N+1}^{!; ;(N+1)} &= G_{i, N}^{!; ;(N)} H_{N, N+1} G_{N+1, N+1}^{!; ;(N+1)} \\
 G_{N+1, j}^{!; ;(N+1)} &= G_{N+1, N+1}^{!; ;(N+1)} H_{N+1, N} G_{N, j}^{!; ;(N)} : 
 \end{aligned} \quad (16)$$

The calculation of the ac conductivities starts with the Kubo formula (15) by setting up a recursion equation for fixed energy  $E$ , width  $L_y = M a$ , and imaginary frequency  $\omega$ , which, e.g., for the longitudinal component reads

$$\begin{aligned}
 e_{xx}(E; \omega; N) &= \frac{e^2}{h M N a^2} S_N^{xx} = \frac{e^2}{h M N a^2} \text{Tr} \sum_{i,j} \frac{X_i^N h}{(h!)^2} x_i G_{ij}^{!; ;+} x_j G_{ji}^{!; ;+} \\
 &\quad + (h!)^2 x_i G_{ij}^{!; ;+} x_j G_{ji}^{!; ;+} + 2i\omega \sum_{i,j} x_i^2 (G_{ij}^{!; ;+} - G_{ji}^{!; ;+}) : 
 \end{aligned} \quad (17)$$

The iteration equation for adding a new slice is given by

$$\begin{aligned}
 S_{N+1}^{xx} &= S_N^{xx} + \text{Tr} A_N R_{N+1} + D_N^1 R_{N+1}^{!; ;+} D_N^2 R_{N+1} \\
 &\quad + B_N R_{N+1}^{!; ;+} D_N^3 R_{N+1}^{!; ;+} D_N^4 R_{N+1}^{!; ;+} C_N R_{N+1}^{!; ;+} : 
 \end{aligned} \quad (18)$$

with  $R_{N+1}^{!; ;+} = G_{N+1, N+1}^{!; ;(N+1)}$ , and a set of auxiliary quantities as defined in the appendix. The coupled iteration equations and the auxiliary quantities are evaluated numerically, the starting values are set to be zero. In addition, coordinate translations are required in each iteration step to keep the origin  $x_{N+1} = 0$  which then guarantees the numerical stability.

## 5 Longitudinal conductivity $\sigma_{xx}(E; \omega)$

In this section we present our numerical results of the longitudinal conductivity as a function of frequency for various positions of the Fermi energy

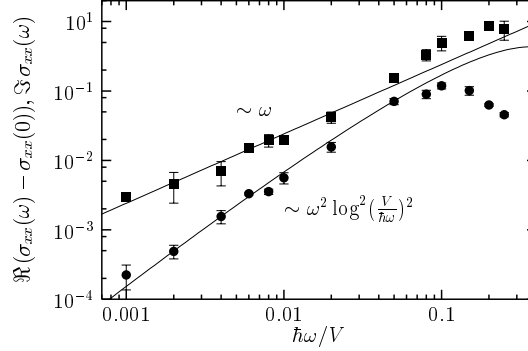


Fig.5. The real (○) and imaginary (■) part of  $\sigma_{xx}(E_F; \omega)$  in units of  $e^2/\hbar$  at  $E_F = V = 3.5$  as a function of frequency. Further parameters are the disorder strength  $W = V = 1.0$ , system width  $L_y = a = 32$  and  $\eta = V = 0.0004$ .

within the lowest Landau band. The real and imaginary parts of  $\sigma_{xx}(E_F; \omega)$  were calculated for several frequencies, but, for the sake of legibility, only four of them are plotted in Fig. 3 versus energy. While the real part exhibits a positive single Gaussian-like peak with maximum  $0.5 e^2/\hbar$  at the critical energy, the imaginary part, which is negative almost everywhere, has a double structure and vanishes near the critical point.  $\sigma_{xx}(E_F; \omega)$  almost looks like the modulus of the derivative of the real part with respect to energy. Plotting  $\sigma_{xx}(E_F; \omega)$  as a function of  $\sigma_{xx}(E_F; \omega)$  (see Fig. 4) we obtain for frequencies  $\omega < \omega_c$  a single, approximately semi-circular curve that, up to a minus sign, closely resembles the experimental results of Hohls et al. [31]. However, for larger  $\omega$  our data points deviate from a single curve.

### 5.1 Frequency dependence of real and imaginary parts

The behaviour of the real and imaginary part of the longitudinal conductivity in the lower tail of the lowest Landau band ( $E = V = 3.5$ ) is shown in Fig. 5. We find for the imaginary part a linear frequency dependence for small  $\omega$  which is, apart from a minus sign, in accordance with (1) [27]. The real part can nicely be fitted to  $\omega^{-2} \log^2 [V/(\hbar\omega)]^2$  in accordance with (1) and  $b = 2$ , but disagrees with the findings in [26] where  $b = 1$  was proposed.

### 5.2 Behaviour of the maximum of $\sigma_{xx}(\omega)$

The frequency dependence of the real part of the longitudinal conductivity peak value was already investigated in [32] where for long-range correlated disorder potentials a non-Drude-like decay was observed. We obtained a similar behaviour also for spatially uncorrelated disorder potentials in a lattice model [61]. In Fig. 6 the difference  $|\sigma_{xx}^p(\omega) - \sigma_{xx}^p(0)|$  is plotted versus frequency in a double logarithmic plot from which a linear relation can be

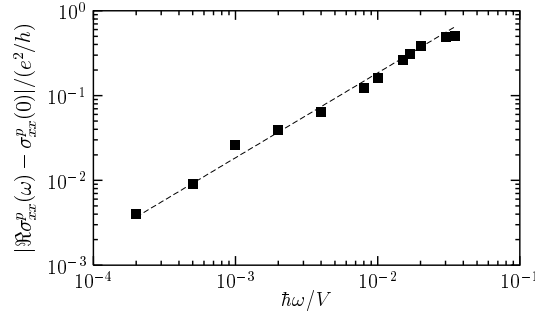


Fig. 6. The non-D rude decrease of the peak value of the longitudinal conductivity as a function of frequency. A linear behaviour of  $|\sigma_{xx}^p(\omega) - \sigma_{xx}^p(0)|$  is clearly observed with  $\sigma_{xx}^p(0) = (e^2/h) = 0.512$  using the following parameters  $E = V = 3.29$ ,  $W = V = 0.1$ ,  $L_y = a = 32$ ,  $\mu = V = 0.0004$

discerned. A linear increase with frequency was found for the imaginary part of the longitudinal conductivity at the critical point as well [61]. The standard explanation for the non-D rude behaviour in terms of long time tails in the velocity correlations, which were shown to exist in a QHE system [32,35], seems not to be adequate in our case. For the uncorrelated disorder potentials considered here, it is not clear whether the picture of electron motion along equipotential lines, a basic ingredient for the arguments in [32], is appropriate.

### 5.3 Scaling of the $\sigma_{xx}(\omega)$ peak width

The scaling of the width of the conductivity peaks with frequency is shown in Fig. 7 where both the  $\sigma_{xx}(\omega)$  peak width expressed in energy and, due to the knowledge of the density of states, in filling factor are shown to follow

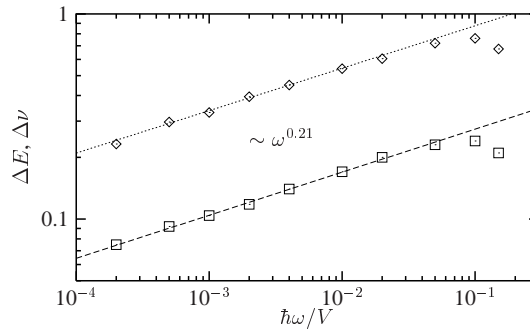


Fig. 7. Frequency scaling of the  $\sigma_{xx}(\omega)$  peak width. The width in energy  $\Delta E$  (2) and the width in filling factor  $\Delta \nu$  (3) show a power-law scaling with an exponent  $\alpha = (\alpha_z)^{-1} = 0.21$

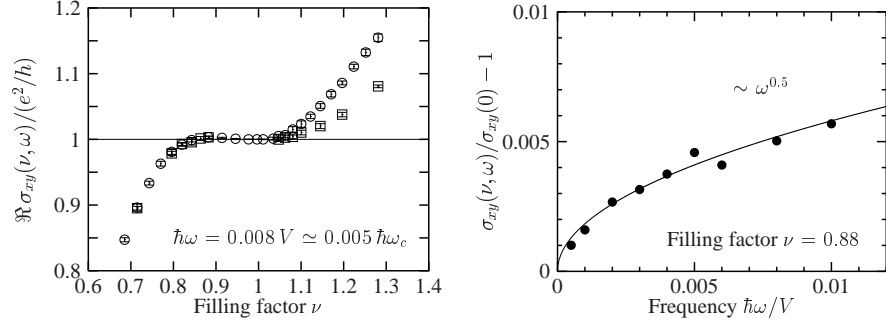


Fig. 8. Frequency dependent Hall-conductivity: The figure on the l.h.s shows  $\sigma_{xy}(!)$  versus filling factor for two system sizes  $L_y/a = 64$  ( ) and  $L_y/a = 128$  ( ). On the r.h.s., the relative deviation of the Hall-conductivity from the dc value,  $\sigma_{xy}(!) = \sigma_{xy}(0) - 1$ , is plotted as a function of frequency for  $\nu = 0.88$

a power-law  $\sigma_{xy}(!) \propto \omega^z$  with  $z = (z)^{-1} = 0.21$  [60]. Taking  $\nu = 2.35$  from [14] we get  $z = 2.026$  close to what is expected for non-interacting electrons. Therefore, the result reported in [42] seems to be doubtful. However, spatial correlations in the disorder potentials as considered in [42] may influence the outcome. Alternatively, one could fix  $z = 2$  and obtain  $\nu = 2.38$  in close agreement with the results from numerical calculations of the scaling of the static conductivity [63] or the localisation length [14].

The experimentally observed values  $\nu = 0.42$  [6] and  $\nu = 0.5 - 0.1$  [12] are larger by a factor of about 2. This is usually attributed to the influence of electron-electron interactions ( $z = 1$ ) which were neglected in the numerical investigations.

## 6 Frequency dependent Hall-conductivity

The Hall-conductivity due to an external time dependent electric field as a function of filling factor is shown in Fig. 8 for system widths  $L_y/a = 64$  and  $L_y/a = 128$ , respectively. While  $\sigma_{xy}(!)$  has already converged for  $E_F$  lying in the upper tail of the lowest Landau band a pronounced shift can be seen in the lower tail of the next Landau band. For  $\nu = 1.3$  a system width of at least  $L_y/a = 192$  was necessary for  $\sigma_{xy}(!)$  to converge. This behaviour originates in the exponential increase of the localisation length with increasing Landau band index. Due to the applied frequency  $\hbar\omega = V = 0.008$  the  $\sigma_{xy}$  plateau is not flat, but rather has a parabola shape near the minimum at  $\nu = 1.0$ , similar to what has been observed in experiment [24]. An example of the deviation of  $\sigma_{xy}(!)$  from its quantised dc value is shown on the right hand side of Fig. 8 where  $\sigma_{xy}(!) = \sigma_{xy}(0) - 1$  is plotted versus frequency for filling factor  $\nu = 0.88$ . A power-law curve  $\sim \omega^{0.5}$  can be fitted to the data points. Using this empirical relation, we find a relative deviation of the order

of  $5 \times 10^6$  when extrapolated down to  $1 \text{ kHz}$ , the frequency usually applied in metrological experiments [21,22,23,24]. Therefore, there is no quantisation in the neighbourhood of integer filling even in an ideal 2d electron gas without contacts, external leads, and other experimental imperfections. Recent calculations, however, show that this deviation can be considerably reduced, even below  $1 \times 10^8$ , if spatially correlated disorder potentials are considered in the model [64].

## 7 Conclusions

The frequency dependent electrical transport in integer quantum Hall systems has been reviewed and the various theoretical developments have been presented. Starting from a linear response expression a method has been demonstrated which is well suited for the numerical evaluation of the real and imaginary parts of both the time dependent longitudinal and the Hall-conductivity. In contrast to the analytical approaches, no further approximations or restrictions such as the position of the Fermi energy have to be considered.

We discussed recent numerical results in some detail with particular emphasis placed on the frequency scaling of the peak width of the longitudinal conductivity emerging at the quantum critical points, and on the quantisation of the ac Hall-conductivity at the plateau. As expected, the latter was found to depend on the applied frequency. The extrapolation of our calculations down to low frequencies resulted in a relative deviation of  $5 \times 10^6$  at  $1 \text{ kHz}$  when spatially uncorrelated disorder potentials are considered. Disorder potentials with spatial correlations, likely to exist in real samples, will probably reduce this pronounced frequency effect.

Our result for the frequency dependence of the  $\sigma_{xx}$  peak width showed power-law scaling,  $\propto \omega^{-1}$ , where  $\omega = (\hbar/\hbar_0)^{-1} = 0.21$  as expected for non-interacting electrons. Therefore, electron-electron interactions have presumably to be taken into account to explain the experimentally observed  $0.5$ . Also, the influence of the spatial correlation of the disorder potentials may influence the value of  $\omega$ .

The frequency dependences of the real and imaginary parts of the longitudinal conductivities, previously obtained analytically for Fermi energies lying deep down in the lowest tail of the lowest Landau band, have been confirmed by our numerical investigation. However, the quadratic behaviour found at low frequencies for the real part of  $\sigma_{xx}(\omega)$  has to be contrasted with the linear frequency dependence that has been proposed for hopping conduction.

Finally, a non-trivial decay of the  $\sigma_{xx}$  peak value with frequency,  $\sigma_{xx}^p(\omega)/\sigma_{xx}^p(0) \propto \omega^{-1}$ , as reported earlier for correlated disorder potentials, has been observed also in the presence of uncorrelated disorder potentials. A convincing explanation for the latter behaviour is still missing.

## Appendix

The iteration equations of the auxiliary quantities (required in (18)) can be written as [62] with  $V_N$   $H_{N,N+1} = H_{N+1,N}^y$

$$A_{N+1} = V_{N+1}^y R_{N+1} A_N + D_N^1 R_{N+1}^{!;+} D_N^2 R_{N+1} V_{N+1} \quad (19)$$

$$B_{N+1} = V_{N+1}^y R_{N+1}^{!;+} B_N - D_N^3 R_{N+1}^+ D_N^4 + D_N^2 R_{N+1} D_N^1 R_{N+1}^{!;+} V_{N+1} \quad (20)$$

$$C_{N+1} = V_{N+1}^y R_{N+1}^+ C_N + D_N^4 R_{N+1}^{!;+} D_N^3 R_{N+1}^+ V_{N+1} \quad (21)$$

$$F_{N+1} = V_{N+1}^y R_{N+1}^{!;+} F_N + D_N^3 R_{N+1}^+ D_N^4 R_{N+1}^{!;+} V_{N+1} \quad (22)$$

$$G_{N+1} = V_{N+1}^y R_{N+1} G_N + D_N^{10} R_{N+1}^{!;+} D_N^{11} R_{N+1} V_{N+1} \quad (23)$$

$$H_{N+1} = V_{N+1}^y R_{N+1}^{!;+} H_N + D_N^{11} R_{N+1} D_N^{10} R_{N+1}^{!;+} V_{N+1} \quad (24)$$

$$D_{N+1}^1 = V_{N+1}^y R_{N+1} D_N^1 R_{N+1}^{!;+} V_{N+1} \quad (25)$$

$$D_{N+1}^2 = V_{N+1}^y R_{N+1}^{!;+} D_N^2 R_{N+1} V_{N+1} \quad (26)$$

$$D_{N+1}^3 = V_{N+1}^y R_{N+1}^{!;+} D_N^3 R_{N+1}^+ V_{N+1} \quad (27)$$

$$D_{N+1}^4 = V_{N+1}^y R_{N+1}^+ D_N^4 R_{N+1}^{!;+} V_{N+1} \quad (28)$$

$$D_{N+1}^5 = V_{N+1}^y R_{N+1} D_N^5 R_{N+1} V_{N+1} \quad (29)$$

$$D_{N+1}^6 = V_{N+1}^y R_{N+1}^+ D_N^6 R_{N+1}^+ V_{N+1} \quad (30)$$

$$D_{N+1}^{10} = V_{N+1}^y R_{N+1} D_N^{10} R_{N+1}^{!;+} V_{N+1} \quad (31)$$

$$D_{N+1}^{11} = V_{N+1}^y R_{N+1}^{!;+} D_N^{11} R_{N+1} V_{N+1} \quad (32)$$

$$D_{N+1}^{14} = V_{N+1}^y R_{N+1}^{!;+} D_N^{14} R_{N+1}^{!;+} V_{N+1} \quad (33)$$

$$D_{N+1}^{15} = V_{N+1}^y R_{N+1}^{!;+} D_N^{15} R_{N+1}^{!;+} V_{N+1} \quad (34)$$

$$D_{N+1}^{16} = V_{N+1}^y R_{N+1} D_N^{16} R_{N+1} V_{N+1} \quad (35)$$

$$E_{N+1}^1 = V_{N+1}^y R_{N+1}^+ E_N^1 + (h!) I R_{N+1}^+ V_{N+1} \quad (36)$$

$$E_{N+1}^2 = V_{N+1}^y R_{N+1} E_N^2 + (h!) I R_{N+1} V_{N+1} \quad (37)$$

$$E_{N+1}^3 = V_{N+1}^y R_{N+1}^{!;+} E_N^3 + (h!) I R_{N+1}^{!;+} V_{N+1} \quad (38)$$

$$E_{N+1}^4 = V_{N+1}^y R_{N+1}^{!;+} E_N^4 + (h!) I R_{N+1}^{!;+} V_{N+1} ; \quad (39)$$

where the auxiliary quantities are defined by

$$A_N = V_N^y \sum_{i,j}^{X^N} G_{Ni} x_i (h!)^2 G_{ij}^{!;+} - 2i''_{ij} I x_j G_{jN} V_N \quad (40)$$

$$B_N = V_N^y \sum_{i,j}^{X^N} G_{Ni}^{!;+} x_i (h!)^2 G_{ij} + 2i''_{ij} I + (h!)^2 G_{ij}^+ x_j G_{jN}^{!;+} V_N \quad (41)$$

$$C_N = V_N^y \sum_{i,j} X^N_{ij} (\hbar!)^2 G_{N\ i}^+ x_i G_{ij}^{!;+} x_j G_{jN}^+ V_N \quad (42)$$

$$F_N = V_N^y \sum_{i,j} X^N_{ij} (\hbar!)^2 G_{N\ i}^{!;+} x_i G_{ij}^+ x_j G_{jN}^{!;+} V_N \quad (43)$$

$$G_N = V_N^y \sum_{i,j} X^N_{ij} (\hbar!)^2 G_{N\ i} x_i G_{ij}^{!;+} x_j G_{jN} V_N \quad (44)$$

$$H_N = V_N^y \sum_{i,j} X^N_{ij} (\hbar!)^2 G_{N\ i}^{!;+} x_i G_{ij} x_j G_{jN}^{!;+} V_N \quad (45)$$

$$D_N^1 = V_N^y \sum_i X^N_i (\hbar!) G_{N\ i} x_i G_{iN}^{!;+} V_N \quad (46)$$

$$D_N^2 = V_N^y \sum_i X^N_i (\hbar!) G_{N\ i}^{!;+} x_i G_{iN} V_N \quad (47)$$

$$D_N^3 = V_N^y \sum_i X^N_i (\hbar!) G_{N\ i}^{!;+} x_i G_{iN}^+ V_N \quad (48)$$

$$D_N^4 = V_N^y \sum_i X^N_i (\hbar!) G_{N\ i}^+ x_i G_{iN}^{!;+} V_N \quad (49)$$

$$D_N^5 = V_N^y \sum_i X^N_i (\hbar!) G_{N\ i} x_i G_{iN} V_N \quad (50)$$

$$D_N^6 = V_N^y \sum_i X^N_i (\hbar!) G_{N\ i}^+ x_i G_{iN}^+ V_N \quad (51)$$

$$D_N^{10} = V_N^y \sum_i X^N_i (\hbar!) G_{N\ i} x_i G_{iN}^{!;+} V_N \quad (52)$$

$$D_N^{11} = V_N^y \sum_i X^N_i (\hbar!) G_{N\ i}^{!;+} x_i G_{iN} V_N \quad (53)$$

$$D_N^{14} = V_N^y \sum_i X^N_i (\hbar!) G_{N\ i}^{!;+} x_i G_{iN}^{!;+} V_N \quad (54)$$

$$D_N^{15} = V_N^y \sum_i X^N_i (\hbar!) G_{N\ i}^{!;+} x_i G_{iN}^{!;+} V_N \quad (55)$$

$$D_N^{16} = V_N^y \sum_i X^N_i (\hbar!) G_{N\ i} x_i G_{iN} V_N \quad (56)$$

$$E_N^1 = V_N^y \sum_i X_i^N (h!) G_{N,i}^+ G_{iN}^+ V_N \quad (57)$$

$$E_N^2 = V_N^y \sum_i X_i^N (h!) G_{N,i} G_{iN} V_N \quad (58)$$

$$E_N^3 = V_N^y \sum_i X_i^N (h!) G_{N,i}^{!+} G_{iN}^{!+} V_N \quad (59)$$

$$E_N^4 = V_N^y \sum_i X_i^N (h!) G_{N,i}^{!;} G_{iN}^{!;} V_N : \quad (60)$$

For the translation of the coordinates  $x_i \rightarrow x_i$  one gets

$$A_N^0 = A_N + H_N^1 - 2aD_N^5 + a^2E_N^2 + aH_N^3 \quad (61)$$

$$B_N^0 = B_N + H_N^2 - H_N^1 + a(H_N^4 - H_N^3) \quad (62)$$

$$C_N^0 = C_N + H_N^2 - 2aD_N^6 + a^2E_N^1 + aH_N^4 \quad (63)$$

$$F_N^0 = F_N - aD_N^4 + 2aD_N^{15} - aD_N^3 - aH_N^4 - a^2E_N^3 \quad (64)$$

$$G_N^0 = G_N + a(D_N^{10} + D_N^{11}) - 2aD_N^{16} + a^2E_N^2 + aH_N^5 \quad (65)$$

$$H_N^0 = H_N - aD_N^{10} + 2aD_N^{14} - aD_N^{11} - aH_N^5 - a^2E_N^4 \quad (66)$$

$$D_N^{1=2^0} = D_N^{1=2} + H_N^3 \quad (67)$$

$$D_N^{3=4^0} = D_N^{3=4} + H_N^4 \quad (68)$$

$$D_N^{5^0} = D_N^5 - aE_N^2 \quad (69)$$

$$D_N^{6^0} = D_N^6 - aE_N^1 \quad (70)$$

$$D_N^{10=11^0} = D_N^{10=11} + H_N^5 \quad (71)$$

$$D_N^{14^0} = D_N^{14} - aE_N^4 \quad (72)$$

$$D_N^{15^0} = D_N^{15} - aE_N^3 \quad (73)$$

$$D_N^{16^0} = D_N^{16} - aE_N^2 ; \quad (74)$$

with the following abbreviations

$$H_N^1 = a(D_N^1 + D_N^2) \quad (75)$$

$$H_N^2 = a(D_N^3 + D_N^4) \quad (76)$$

$$H_N^3 = aV_N^y (R_N^{!+} - R_N) V_N \quad (77)$$

$$H_N^4 = aV_N^y (R_N^{!+} - R_N^+) V_N \quad (78)$$

$$H_N^5 = aV_N^y (R_N^{!;} - R_N) V_N : \quad (79)$$



## References

1. B. Huckestein: Rev. Mod. Phys. 67, 357 (1995)
2. S. L. Sondhi, S. M. Girvin, J. P. Carini, D. Shahar: Rev. Mod. Phys. 69 (1), 315 (1997)
3. F. Kuchar, R. Meisels, G. Weinmann, W. Schlapp: Phys. Rev. B 33 (4), 2956 (1986)
4. J. I. Lee, B. B. Goldberg, M. Heiblum, P. J. Stiles: Solid State Commun. 64 (4), 447 (1987)
5. I. E. Batov, A. V. Polisskii, M. I. Reznikov, V. I. Talyanskii: Solid State Commun. 76 (1), 25 (1990)
6. L. W. Engel, D. Shahar, C. Kurdak, D. C. Tsui: Phys. Rev. Lett. 71 (16), 2638 (1993)
7. N. Q. Balaban, U. Meirav, I. Bar-Joseph: Phys. Rev. Lett. 81 (22), 4967 (1998)
8. W. Belitsch, R. Meisels, F. Kuchar, G. Hein, K. Pierz: Physica B 249 (251), 119 (1998)
9. R. Meisels, F. Kuchar, W. Belitsch, G. Hein, K. Pierz: Physica B 256-258, 74 (1998)
10. F. Kuchar, R. Meisels, B. Kramer: Advances in Solid State Physics 39, 231 (1999)
11. D. Shahar, L. W. Engel, D. C. Tsui: In High Magnetic Fields in the Physics of Semiconductors, edited by D. Heinan (World Scientific Publishing Co., Singapore, 1995): pp. 256(259
12. F. Hohls, U. Zeitler, R. J. Haug, R. Meisels, K. Dybko, F. Kuchar: cond-mat/0207426 (2002)
13. B. Huckestein, B. Kramer: Phys. Rev. Lett. 64 (12), 1437 (1990)
14. B. Huckestein: Europhysics Letters 20 (5), 451 (1992)
15. S. Koch, R. J. Haug, K. v. Klitzing, K. Ploog: Phys. Rev. Lett. 67, 883 (1991)
16. D. H. Lee, Z. Wang: Phys. Rev. Lett. 76 (21), 4014 (1996)
17. S. R. E. Yang, A. H. MacDonald: Phys. Rev. Lett. 70 (26), 4110 (1993)
18. B. Huckestein, M. Backhaus: Phys. Rev. Lett. 82 (25), 5100 (1999)
19. Z. Wang, M. P. A. Fisher, S. M. Girvin, J. T. Chalker: Phys. Rev. B 61 (12), 8326 (2000)
20. Z. Wang, S. Xiong: Phys. Rev. B 65, 195316 (2002)
21. F. Delahaye: J. Appl. Phys. 73, 7914 (1993)
22. F. Delahaye: Metrologia 31, 367 (1994/95)
23. S. W. Chua, A. Hartland, B. P. Kibble: IEEE Trans. Instrum. Meas. 48, 309 (1999)
24. J. Schurr, J. Melcher, A. von Campenhausen, G. Hein, F.-J. Ahlers, K. Pierz: Metrologia 39, 3 (2002)
25. R. Joynt: J. Phys. C: Solid State Phys. 18, L331 (1985)
26. W. Apel: J. Phys.: Condens. Matter 1, 9387 (1989)
27. O. V. Iehweger, K. B. Efetov: J. Phys.: Condens. Matter 2 (33), 7049 (1990)
28. O. V. Iehweger, K. B. Efetov: J. Phys.: Condens. Matter 3 (11), 1675 (1991)
29. O. V. Iehweger, K. B. Efetov: Phys. Rev. B 44 (3), 1168 (1991)
30. D. G. Polyakov, B. I. Shklovskii: Phys. Rev. B 48 (15), 11167 (1993)
31. F. Hohls, U. Zeitler, R. J. Haug: Phys. Rev. Lett. 86 (22), 5124 (2001)
32. B. M. Gamme, W. Brenig: Phys. Rev. B 53 (20), R13279 (1996)
33. A. MacInnon: Z. Phys. B 59, 385 (1985)

34. F.Evers, W.Brenig: Z.Phys.B 94, 155 (1994)
35. W.Brenig, B.M.Gammel, P.Kratzer: Z.Phys.B 103, 417 (1997)
36. B.Huckestein, L.Schweitzer: In High Magnetic Fields in Semiconductor Physics III: Proceedings of the International Conference, Würzburg 1990, edited by G.Landwehr (Springer Series in Solid-State Sciences 101, Springer, Berlin, 1992): pp. 84{88
37. W.Pook, M.Jan en: Z.Phys.B 82, 295 (1991)
38. B.Huckestein, B.Kramer, L.Schweitzer: Surface Science 263, 125 (1992)
39. M.Jan en: International Journal of Modern Physics B 8 (8), 943 (1994)
40. J.T.Chalker, G.J.Daniell: Phys. Rev. Lett. 61 (5), 593 (1988)
41. B.Huckestein, L.Schweitzer: Phys. Rev. Lett. 72 (5), 713 (1994)
42. Y.Avishay, J.M.Luck: preprint, cond-mat/9609265 (1996)
43. T.Ando: J. Phys. Soc. Jpn. 53 (9), 3101 (1984)
44. G.Jug, K.Ziegler: Phys. Rev. B 59 (8), 5738 (1999)
45. A.W.Ludwig, M.P.A.Fisher, R.Shankar, G.Grinstein: Phys. Rev. B 50, 7526 (1994)
46. K.Ziegler: Phys. Rev. B 55 (16), 10661 (1997)
47. A.Mackinnon: J. Phys. C 13, L1031 (1980)
48. A.Mackinnon, B.Kramer: Z.Phys.B 53, 1 (1983)
49. A.Mackinnon, B.Kramer: Phys. Rev. Lett. 47 (21), 1546 (1981)
50. A.Mackinnon, B.Kramer: In Lecture Notes in Physics, edited by G.Landwehr (Springer-Verlag, Berlin, Heidelberg, New York, Tokyo, 1982): pp. 74{86
51. L.Schweitzer, B.Kramer, A.Mackinnon: J. Phys. C 17, 4111 (1984)
52. T.Koschny, H.Potempa, L.Schweitzer: Phys. Rev. Lett. 86 (17), 3863 (2001)
53. B.Kramer, L.Schweitzer, A.Mackinnon: Z.Phys.B -Condensed Matter 56, 297 (1984)
54. L.Schweitzer, B.Kramer, A.Mackinnon: Z.Phys.B 59, 379 (1985)
55. C.Villagonzalo, R.A.Romer, M.Schreiber, A.Mackinnon: Phys. Rev. B 62, 16446 (2000)
56. T.Saso, C.I.Kin, T.Kasua: J. Phys. Soc. Jap. 52, 1888 (1983)
57. T.Saso: J. Phys. C 17, 2905 (1984)
58. B.M.Gammel: Ph.D. Thesis (Technical University Munich) (1994)
59. B.M.Gammel, F.Evers: unpublished report, 10 pages (1999)
60. A.Baker, L.Schweitzer: Ann. Phys. (Leipzig) 8, SI-21 (1999)
61. A.Baker, L.Schweitzer: In Proc. 25th Int. Conf. Phys. Semicond., Osaka 2000, edited by N.Miura, T.Ando (Springer, Berlin, 2001): vol. 78 of Springer Proceedings in Physics: pp. 975{976
62. A.Baker, L.Schweitzer: PTB-report, unpublished, 94 pages (2002)
63. B.M.Gammel, W.Brenig: Phys. Rev. Lett. 73 (24), 3286 (1994)
64. L.Schweitzer: to be published (2003)